Neurobiology of Aging 67 (2018) 148–158

Contents lists available at ScienceDirect

Neurobiology of Aging

journal homepage: www.elsevier.com/locate/neuaging

Evidence of Wnt/β-catenin alterations in brain and bone of a tauopathy mouse model of Alzheimer's disease

Christine M. Dengler-Crish [a,*], Hope C. Ball [b], Li Lin [a], Kimberly M. Novak [a], Lisa Noelle Cooper [b]

[a] Department of Pharmaceutical Sciences, Northeast Ohio Medical University, Rootstown, OH, USA
[b] Department of Anatomy & Neurobiology, Northeast Ohio Medical University, Rootstown, OH, USA

ARTICLE INFO

Article history:
Received 24 January 2018
Received in revised form 17 March 2018
Accepted 17 March 2018
Available online 23 March 2018

Keywords:
Tauopathy
Alzheimer's disease
Wnt proteins
Bone mineral density
Beta catenin
Neurodegeneration

ABSTRACT

Low bone mineral density (BMD) is a significant comorbidity in Alzheimer's disease (AD) and may reflect systemic regulatory pathway dysfunction. Low BMD has been identified in several AD mouse models selective for amyloid-β or tau pathology, but these deficits were attributed to diverse mechanisms. In this study, we identified common pathophysiological mechanisms accounting for bone loss and neurodegeneration in the htau mouse, a tauopathy model with an early low BMD phenotype. We investigated the Wnt/β-catenin pathway—a cellular signaling cascade linked to both bone loss and neuropathology. We showed that low BMD persisted in male htau mice aged from 6 to 14 months, remaining significantly lower than tau-null and C57BL/6J controls. Osteogenic gene expression in female and male htau mice was markedly reduced from controls, indicating impaired bone remodeling. In both the bone and brain, htau mice showed alterations in Wnt/β-catenin signaling genes suggestive of increased inhibition of this pathway. These findings implicate dysfunctional Wnt signaling as a potential target for addressing bone loss in AD.

1. Introduction

Skeletal fragility has been recognized as a clinical comorbidity in Alzheimer's disease (AD) for over 20 years (Johansson and Skoog, 1996; Looker et al., 2012; Melton et al., 1994). Low bone mineral density (BMD) and its clinical sequelae, osteoporosis, occur at twice the rate in AD patients as in healthy, elderly adults (Johansson and Skoog, 1996; Looker et al., 2012). These low bone mass conditions weaken the skeleton and increase likelihood of bone fractures, and in patients with AD, this poses significant complications. AD patients who experience a bone fracture event are at an increased risk of disability, decreased quality of life, and hastened mortality (Amouzougan et al., 2017; Bonafede et al., 2016; Melton et al., 1994; Tamimi et al., 2012). As a comorbidity in AD, low BMD occurs independently of sex, age, body mass index, physical activity level, and disease stage (Loskutova et al., 2009; Melton et al., 1994; Weller and Schatzker, 2004; Zhao et al., 2012; Zhou et al., 2011)—making it a challenge to find an obvious factor that accounts for it in this neurodegenerative disorder. Most notably, low BMD has even been used to predict risk of dementia in some populations years before diagnostic confirmation of AD, suggesting that bone health may be affected at presymptomatic stages (Chang et al., 2014; Sohrabi et al., 2015; Tan et al., 2005; Zhou et al., 2011, 2014).

Analogous to this clinical comorbidity, low BMD phenotypes are manifested in several transgenic mouse strains used to model humanized AD neuropathology. These strains include htau (Dengler-Crish et al., 2017), amyloid precursor protein (APP)/presenilin 1 mutant (Peng et al., 2014; Yang et al., 2011), and Swedish mutation APP (Cui et al., 2011; Xia et al., 2013) mice. The strains in which bone loss is noted are quite interesting because htau mice express only one form of AD-like pathology (i.e., tauopathy) and APP-mutant mice more dominantly express amyloid pathology: 2 distinct neuropathological mechanisms in AD. Consistency of a low BMD phenotype across these strains indicates a close relationship between degeneration of brain and bone regardless of pathological specificity. Therefore, identification of common mechanistic factors supporting bone loss in both of these models may provide important information on much needed therapeutic targets for addressing this comorbidity in AD.

Bone loss comorbid with neurodegenerative conditions may reflect either neural dysfunction in bone regulatory structures (Oury et al., 2010; Yadav et al., 2009), detrimental peripheral effects on bone (Kajimura et al., 2013), or a combination of both (Ross et al., 2018;

* Corresponding author at: Department of Pharmaceutical Sciences, Northeast Ohio Medical University, 4209 State Route 44, Rootstown, OH 44272. Tel.: +1 330 325 6598; fax: +1 330 325 5936.
E-mail address: ccrish@neomed.edu (C.M. Dengler-Crish).

0197-4580/$ – see front matter © 2018 Elsevier Inc. All rights reserved.
https://doi.org/10.1016/j.neurobiolaging.2018.03.021

Shi et al., 2010). Bone is a dynamic tissue that shares a number of regulatory signaling pathways with brain tissue that are relevant to degenerative disorders. For example, triggering receptor expressed on myeloid cells-2 (TREM2) is currently an important molecular target in AD research (see Bemiller et al., 2017). TREM2 is expressed on microglia in the nervous system (Jay et al., 2015), where it is shown to play a role in neuroprotection (Bemiller et al., 2017). It is also expressed on bone-specific macrophages (osteoclasts) where it functions as a negative regulator of mineral resorption during normal bone remodeling processes, thus facilitating bone formation (Otero et al., 2012). Mutations in the TREM2 gene have been linked with increased risk of late-onset AD (Guerreiro et al., 2013; Jonsson et al., 2013), bone loss (Otero et al., 2012), and the neurodegenerative Nasu-Hakola disease that produces both senile dementia and osteoporotic bone cysts (Paloneva et al., 2000).

TREM2 activates the canonical Wnt/β-catenin intracellular signaling pathway (Zheng et al., 2017), which is a major regulator of cellular function in most tissues of the body (including bone and brain). The canonical Wnt pathway (schematically described in Fig. 1) activates transcriptional coregulator β-catenin, which is a principle driver of bone formation (reviewed in Krishnan et al., 2006) and mediator of synaptogenesis and neurogenesis in the brain (reviewed in Oliva et al., 2013). Perturbations in Wnt/βcat signaling have been extensively characterized for their contributions to skeletal defects (Korvala et al., 2012; Westendorf et al., 2004), and there is growing evidence that genetic mutations leading to deficient activity of the Wnt/βcat pathway increase the risk of developing AD (Alarcón et al., 2013; Zhang et al., 1998). Therefore, vulnerabilities within the canonical Wnt pathway provide attractive target mechanisms that could account for bone loss comorbid with AD.

In the present study, we sought evidence of alterations in canonical Wnt signaling in the bone and brain of htau mice. Htau mice express pathologically phosphorylated conformations of the microtubule-stabilizing protein tau, which destabilize the neuronal cytoskeleton and assemble into neurofibrillary tangles akin to human AD (Andorfer et al., 2003). Previously, we characterized a robust, low BMD phenotype in this strain present from 3 to 6 months of age, a time when the murine skeleton exhibits rapid, anabolic growth (Dengler-Crish et al., 2017). In this study, we expanded our characterization of htau bone density into older mice across 6–14 months of age—a time of skeletal maturity and stable, homeostatic bone growth more comparable to bone remodeling processes experienced by aging adult humans (Gargiulo et al., 2014; Watanabe and Hishiya, 2005). Adding a powerful contrast to this, we compared changes in BMD and Wnt signaling with C57BL/6J mice, a strain known to exhibit age-related osteoporotic bone loss unrelated to neurodegeneration (Beamer et al., 1996; Watanabe and Hishiya, 2005). This enabled us to determine if skeletal and molecular signaling changes were unique to the AD model. Our data revealed significant skeletal density deficits and evidence of impaired bone remodeling in aged htau mice that exceeded those of control mice. Deficits in skeletal integrity/remodeling coincided with multiple alterations in canonical Wnt signaling, both

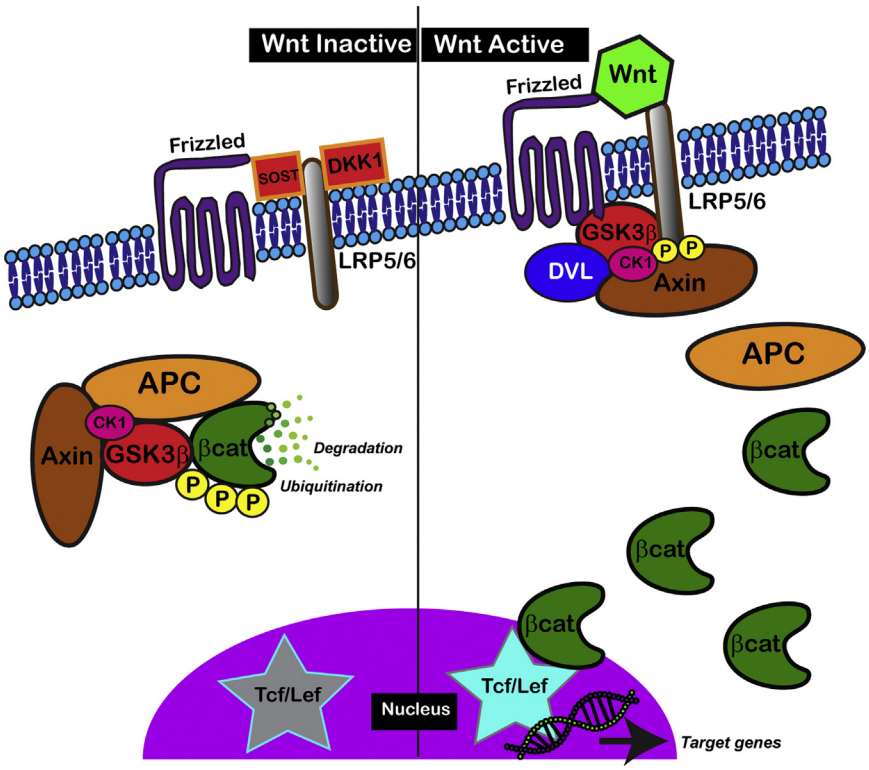

Fig. 1. Schematic representation of the Wnt/β-catenin (βcat) signaling pathway during inactive and active states. Inactive state (left): The constituent inactivity of βcat is maintained by a destruction complex composed of axin, tumor suppressor adenomatous polyposis coli (APC), casein kinase-1 (CK-1), and glycogen synthesis kinase (GSK)3β (Aberle et al., 1997; Clevers and Nusse, 2012). GSK3β phosphorylates βcat, marking it for ubiquitination and proteasomal degradation, causing overall inhibition of its activity in the cell (Liu et al., 2002). In addition, this pathway can be actively inhibited by endogenous antagonists such as the secreted glycoproteins dickkopf homologue I (DKK1) or sclerostin (SOST), which bind to the low-density lipoprotein-related receptor protein (LRP5/6) Wnt co-receptor (Bourhis et al., 2011; Mao et al., 2001). Active state (right): Wnt activators (e.g., Wnt3a, Wnt5, Wnt7a,Wnt7b, and Wnt8) bind and activate coreceptors frizzled and LRP5/6, triggering the recruitment of the protein disheveled (DVL), which assists in disrupting the destruction complex (Willert et al., 1999). Coactivation of frizzled/LRP5/6 enables phosphorylation of GSK3β at its inhibitory site, serine 9, thereby suppressing its phosphorylation/restriction of βcat (Zhao et al., 2015). Without GSK3β and the destruction complex to quash it, free βcat accumulates in the cytosol, translocates to the nucleus, and can activate the TCF/LEF (T-cell factor/lymphoid enhancer–binding factor) family of DNA binding proteins, which facilitate target gene transcription or suppression (Arce et al., 2006).

peripherally in the bone and in the central nervous system. Taken together, this evidence suggests that integrative studies of the bone and brain may offer novel insights into a potentially common molecular regulator responsible for degeneration in both systems.

2. Materials and methods

2.1. Subjects

Male and female htau mice (B6.Cg-Mapt $^{tm1(GFP)}$ Tg(MAPT) 8cPdav/J strain on a C57BL/6J background) were used in this study. Htau mice are homozygous for a targeted deletion of the mouse microtubule-associated protein tau (MAPT) allele and hemizygous for insertion of a humanized MAPT (hMAPT) transgene. The hMAPT transgene triggers expression of all 6 human tau isoforms in the absence of endogenous mouse MAPT (Andorfer et al., 2003). Htau mice are a clinically relevant disease model because they express the 3R/4R tau isoform pattern that is associated with late-onset human AD (Panda et al., 2003). Around 3 months, htau mice exhibit an osteoporotic phenotype that coincides with elevated ptau levels in brainstem regions associated with serotonergic regulation of skeletal remodeling (Dengler-Crish et al., 2017). Pervasive ptau and neurofibrillary tangle pathology are present in other brain regions such as the hippocampus and cortex by 6–9 months (Andorfer et al., 2003; Komuro et al., 2015; Polydoro et al., 2009).

The primary control group consisted of age- and sex-matched C57BL/6J (C57) mice, the background strain on which htau were developed. Notably, C57 mice exhibit age-related osteoporotic bone loss (Beamer et al., 1996; Watanabe and Hishiya, 2005), making them an apt contrast for deleterious changes in the htau skeleton. For an additional comparison, age- and sex-matched littermates of htau mice that are true tau knock-outs devoid of endogenous mouse MAPT and are noncarriers of the hMAPT transgene were also studied. While these tau-null mice controlled for endogenous MAPT manipulation, their lack of any MAPT (mouse or human) produces developmental phenotypes unrelated to AD, making them poor primary controls (Dengler-Crish et al., 2017; Geiszler et al., 2016). Thirty mice were used for the experiment (5 mice per sex per strain) and the study began at 6 months of age, followed by sacrifice at 14 months. A separate cohort consisting of 24 two-month-old htau, tau null, and C57 mice (4 mice per sex per strain group) was used to provide replication data across the 2- to 5-month skeletal growth period that was previously characterized in Dengler-Crish et al. (2017). Skeletal changes across this highly anabolic growth period were compared with changes that occurred in the mature homeostatic bone remodeling phase (6–14 months) targeted in the present study.

All mice were obtained from breeding colonies at the Northeast Ohio Medical University Comparative Medicine Unit and were housed in the same room under identical environmental conditions. Breeding stocks of htau mice were originally obtained from Jackson Laboratories (stock #005491), and automated genotyping of transgenic offspring was performed by Transnetyx (Cordova, TN) using real-time polymerase chain reaction (PCR). All procedures using mice were approved in accordance with the Northeast Ohio Medical University Institutional Animal Care and Use Committee.

2.2. Bone densitometry

Bone density was measured monthly using dual emission x-ray absorptiometry (DEXA) on a Lunar PIXImus (GE Healthcare) scanner. DEXA is a high-throughput radiographic method for accurately measuring bone density and body composition in live animals (Fuchs et al., 2013). Mice were weighed and anesthetized with 2.5% inhaled isoflurane vapor to provide immobilization and were then placed onto the PIXImus platform where they received a 5-minute DEXA scan as previously described (Dengler-Crish et al., 2017). Analysis performed using PIXImus software (GE Healthcare/Lunar) provided quantification of overall skeletal BMD as well as BMD measurements of targeted regions of interest that included the femur and lumbar spine. These bone sites reflect dominance of specific skeletal envelopes with different metabolic properties (i.e., cortical bone-dominant femur or trabecular bone-dominant vertebrae) and enabled determination of any phenotypic effects specific to bone type. Percent body fat composition was also measured using the PIXImus software and was used along with body mass data to determine any effects of overall body size/composition on bone health. Detailed descriptions of these methods including regions of interest delineations are reported in Dengler-Crish et al. (2017).

2.3. Tissue collection

After the final DEXA scans were performed at 14 months of age, mice were sacrificed via decapitation under inhaled isoflurane (3.5%) anesthesia. The femur and tibia were dissected from the lower limbs, and bones were stabilized in RNAlater (ThermoFisher Scientific, Waltham, MA) and frozen at −80°C until analysis. Hippocampus and brainstem regions centered around the dorsal raphe nuclei were dissected from mouse brains and frozen immediately in liquid nitrogen. Brain samples were stored at −80°C until analysis.

2.4. RNA isolation/cDNA synthesis for quantitative real-time PCR

Total RNA was isolated from mouse femora and tibiae under RNAse-free conditions following recommended protocols for TRI Reagent (ThermoFisher) and treated with Turbo DNA-free (ThermoFisher) to remove DNA contaminants. Extracted RNA was quantified on a NanoDrop 2000c spectrophotometer (NanoDrop, Wilmington, DE), and RNA integrity was assessed via visualization of extracted RNAs on an ethidium bromide–stained 1% agarose gel. cDNA and reverse transcriptase controls were synthesized using the High-Capacity cDNA Reverse Transcription kit (ThermoFisher). Synthesized cDNAs were then normalized to 50 ng total RNA. For brain samples, total RNA was isolated from hippocampal and brainstem homogenates using IBI isolate (IBI Scientific, Peosta, IA), and 900 ng of total RNA was used to synthesize cDNA with Verso cDNA synthesis kit (ThermoFisher).

In bone tissue, expression profiles of the following osteogenic genes were used to assess positive bone formation and structural skeletal integrity: collagen type Iα1 (*Col1a1*), a high abundance fibril-forming collagen associated with bone maturation (Chaplin et al., 2015) and collagen type Vα1 (*Col5a1*), a low abundance collagen that confers strength to bone tissue (Wu et al., 2010). Expression profiles were determined for Wnt-related genes selected to represent extracellular and intracellular (including receptor and nuclear) signaling levels of the pathway, as well as components involved in bone formation and neuroprotection (refer to Fig. 1). Bone-specific Wnt genes that were assessed included sclerostin (*Sost*), a secreted polypeptide and Wnt antagonist that promotes bone resorption and inhibits formation; and the Wnt/βcat–activated runt-related transcription factor 2 (*Runx2*) that promotes bone formation (Komori, 2010). Assessment of genes associated with Wnt signaling components included βcat (*Catenin beta-1* or *CTNNB1*), low-density lipoprotein–related receptor protein 5 (*Lrp5*; predominantly form in bone), *Lrp6* (predominant form in brain), Wnt antagonist Dickkopf homologue 1 (*Dkk1*), endogenous Wnt activators *Wnt3a* (ligand associated with bone formation) and *Wnt7a* (ligand involved in synaptogenesis/neuroprotection),

and DNA binding protein T-cell factor/lymphoid enhancer binding factor *Tcf4 (Tcf7Lef2)*. *Tcf4* was targeted because it is known to activate bone-forming osteoblasts (Bennett et al., 2005) as well as an important role in the suppression of the β-site APP cleaving enzyme 1 (*Bace1*) promotor, which, when uninhibited, contributes to the neurotoxic pathological amyloid-β (Aβ) load characteristic of AD (Parr et al., 2015; Tapia-Rojas et al., 2016). All genes, their functional significance, location in which they were assayed, and associated primer sequences are described in Table 1.

Quantitative real-time PCR reactions were run in duplicate on either an ABI 7900-HT or QuantStudio 6 Flex PCR system (Applied Biosystems, CA) using PowerUp SYBR Green PCR Master Mix (ThermoFisher). Relative target mRNA expression levels in brain samples were normalized to GAPDH reference using the ΔΔCt method. ΔCt values of target genes from C57 mice were used as a calibrator to determine the relative fold change in gene expression between the 3 strain groups. If preliminary analysis revealed sex differences for a particular gene, then data were recalibrated using female C57 values. For analysis of bone tissue, we used a validated method of absolute quantitative real-time PCR (Ball et al., 2013, 2016) to minimize complications associated with housekeeping gene variance, given the novelty of our comparisons of Wnt gene expression in bone across transgenic mouse strains (Bustin, 2002; Fernandes et al., 2008). For each gene target, dilution curves and linear regression equations were generated for use in osteogenic expression analyses, and significance of threshold cycle (Ct) values and amplification efficiencies were calculated (Yuan et al., 2007).

2.5. Statistical analysis

For DEXA-obtained variables, sex and strain group (htau, tau null, and C57) differences in overall skeletal BMD across 6–14 months were analyzed by factorial multivariate analysis of variance (MANOVA). The MANOVA method was used for this particular analysis because it enabled sex-by-strain comparisons for each monthly BMD measurement while compensating for any sphericity violations in the data. Main effects for sex and strain group were determined and qualified by any significant interactions between the 2 variables. When significant main effects of sex or interactions were present, data files were split by sex and analyzed independently for strain differences (Dengler-Crish et al., 2017) using univariate analysis of variance (ANOVAs) and Bonferroni-corrected planned comparisons.

To create a consolidated set of variables representing aggregate changes over the entire homeostatic bone remodeling period, monthly values for total skeletal BMD, femoral BMD, lumbar BMD, body mass, and percent body fat were each averaged across 6–14 months. Sex by strain differences in each of these aggregate variables were assessed with factorial ANOVA models. Follow-up analyses were conducted as described previously with the addition of planned comparisons between males and females within each strain in response to any significant sex effects or interactions. In the absence of significant sex main effects or interactions, data for that variable were collapsed across strain for further comparisons. Statistics are only reported for significant main effects when interactions were absent. Estimates of effect size for main effects and interactions of omnibus analyses are presented as η^2, which describes the percent of group variance that can be attributed to the experimental condition (Warner, 2013).

Based on methodological differences, gene expression variables are presented as either transcript copy number (bone samples) or relative expression/fold change (brain samples). For each gene and site of expression (i.e., bone, hippocampus, brainstem), 2-way (sex by strain) ANOVAs were used to establish differences between groups, and univariate ANOVAs with either Bonferroni or Tukey's honestly significant difference tests were used to follow-up significant main effects and interactions. Wherever sex effects were absent in the omnibus tests, data were pooled across strains to increase statistical power.

3. Results

3.1. Low BMD phenotype in htau mice persists in a sex-dependent manner across homeostatic remodeling phase

Composite results for overall skeletal BMD are presented in Fig. 2. Data for the 2- to 5-month anabolic bone growth period were obtained from a separate replication study; data from 6 to 14 months are plotted from the present study. Replication data were consistent with those reported in Dengler-Crish et al. (2017),

Table 1
Osteogenic (bone formation–promoting) and Wnt pathway–associated genes, their function, site targeted for expression, and primer pair sequences

Target gene	Function	Site	Primer sequence 5′3′	
CTNNB1(*β-Catenin*)	Wnt signaling: transcriptional coregulator; promotes bone formation and neuroprotective effects	Brain, bone	Fwd	CCATCTTAAGCCCTCGCTCG
			Rev	GCTGAGCTTCAGGTACCCTC
Col1a1	Osteogenic: promotes bone formation; bone maturation	Bone	Fwd	CTGGCGGTTCAGGTCCAAT
			Rev	TTCCAGGCAATCCACGAGC
Col5a1	Osteogenic: promotes bone formation/confers bone strength	Bone	Fwd	CTTCGCCGCTACTCCTGTTC
			Rev	CCCTGAGGGCAAATTGTGAAAA
Dkk1	Wnt/βcat antagonist: associated with bone loss and AD pathology	Brain, bone	Fwd	CTCATCAATTCCAACGCGATCA
			Rev	GCCCTCATAGAGAACTCCCG
Lrp5	Wnt coreceptor (predominant form in bone): inhibits GSK3β and increases β-catenin activity	Bone	Fwd	GCAAGAAGCTGTACTGGACG
			Rev	GGCCCTTGGCTGGTCC
Lrp6	Wnt coreceptor (predominant form in the brain): inhibits GSK3β and increases β-catenin activity	Brain	Fwd	TTGTTGCTTTATGCAAACAGACG
			Rev	GTTCGTTTAATGGCTTCTTCGC
Runx2	Osteogenic/Wnt signaling: transcription factor that promotes bone formation	Bone	Fwd	CCAACCGAGTCATTTAAGGCT
			Rev	GCTCACGTCGCTCATCTT
Sost	Local (bone) Wnt/β-Catenin antagonist; secretion product sclerostin inhibits bone formation and promotes bone resorption	Bone	Fwd	AGCCTTCAGGAATGATGCCAC
			Rev	CTTTGGCGTCATAGGGATGGT
Tcf7Lef2 (*TCF4*)	DNA-binding protein with neuroprotective effects; it has binding site for osteogenic *Runx*2 transcription factor	Brain	Fwd	ACCGCCCGAACCTATCTTCA
			Rev	GAACGAGCATCCTTGAGGGT
Wnt3a	Wnt/β-catenin agonist: promotes bone formation and neuroprotection	Bone	Fwd	ACCTGTGAGGGTCTCCTACC
			Rev	TCTCCATTTGAGCCCTGTCG
Wnt7a	Wnt/β-catenin agonist: promotes synaptogenesis and proper neural function	Brain	Fwd	TGAACTTACACAATAACGAGGCG
			Rev	GTGGTCCAGCACGTCTTAGT

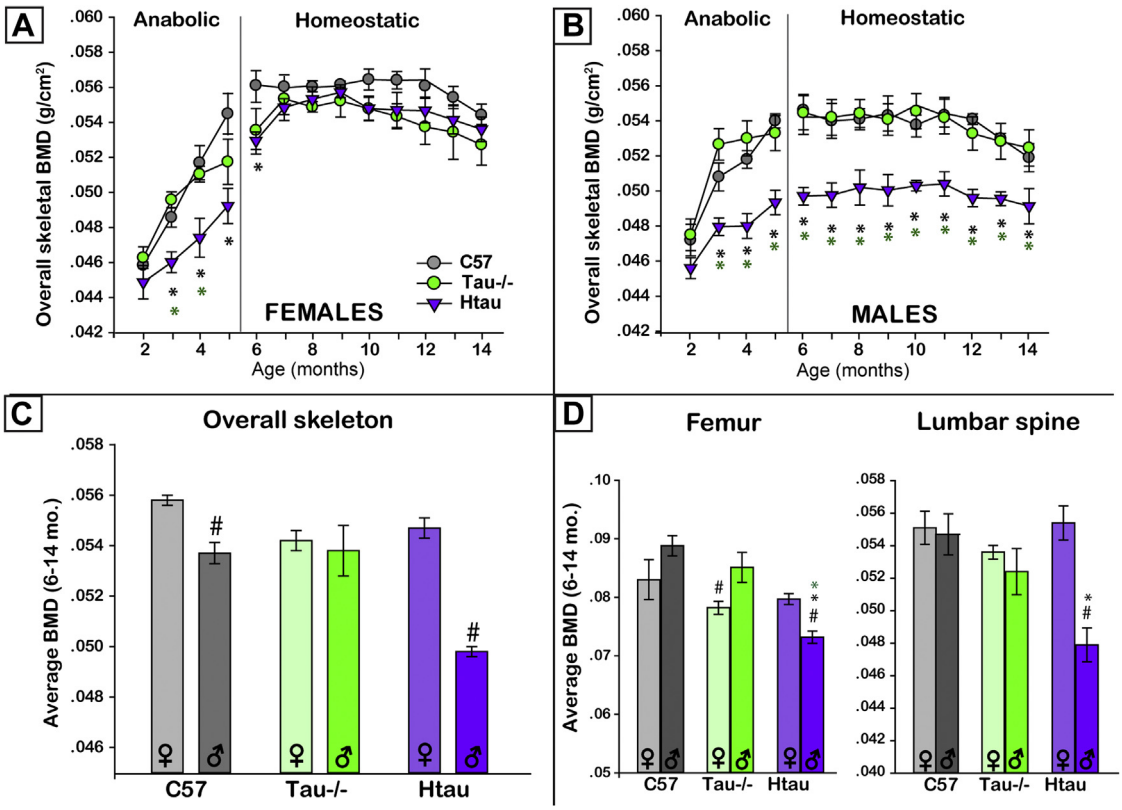

Fig. 2. Bone mineral density (BMD) measured by DEXA across age in htau mice and controls. (A and B) Average monthly BMD measured from overall skeleton in control C57BL/6J (C57; gray circle), tau null (−/−; green circle), and htau (purple triangle) strain groups graphed separately for female (A) and male (B) mice. Reference BMD data from a separate sample of mice are plotted for the 2- to 5-month anabolic skeletal growth phase and provide a replication of findings previously reported in Dengler-Crish et al. (2017). BMD data from the target observation period of 6–14 months represent bone growth during a homeostatic phase of skeletal remodeling. Black asterisks indicate statistically significant differences between htau and C57; green asterisks indicate significant differences between htau and tau −/− mice ($p < 0.05$); error bars depict standard error of the mean (s.e.m). (A) Among females, htau mice initially exhibit reduced BMD compared to controls during the anabolic skeletal growth phase from 3 to 6 months of age but reach control densities by 7 months with no further significant differences up to 14 months. (B) Among males, htau BMD is significantly reduced from C57 and tau −/− siblings throughout early anabolic growth, and this reduction is sustained for the duration of the homeostatic growth phase (6–14 months of age). (C) Differences in overall skeletal density averaged over the entire homeostatic bone remodeling period are shown for female (♀) and male (♂) C57 (gray bars), tau −/− (green bars), and htau (purple bars) mice. Male C57 had a 4% reduction in BMD from female C57, and male htau mice exhibited a 9% reduction bone mass from female htau. # symbols indicate statistically significant sex differences ($p < 0.05$); error bars depict s.e.m. (D) Mean femoral (left) and lumbar spine (right) BMD averaged over 6–14 months. BMD at either site did not differ among female mice. Among males, htau mice had reduced femoral and lumbar BMD compared to C57 mice (black asterisk = $p < 0.05$) but only differed from tau-null siblings in femoral density (green asterisk = $p < 0.05$). When compared to female conspecifics, male htau displayed significantly lower BMD at both bone sites. # symbols indicate significant sex differences of ($p < 0.05$). Error bars show s.e.m.

confirming significant differences in overall BMD from 3–5 months of age in female and male htau mice compared to C57 controls and tau nulls. For the homeostatic skeletal remodeling period (6–14 months), MANOVA results indicated significant main effects for sex and strain, which were qualified by significant interactions for BMD measurements from 7–14 months (see Appendix A for individual statistics at each month). At 6 months, htau BMD was significantly reduced from C57 (Bonferroni-corrected p =0.001) and tau nulls (Bonferroni-corrected p = 0.02), $F_{2,27}$ =9.87, p =0.001. Follow-up comparisons from ages 7–14 months were conducted separately by sex. From 7 to 14 months, female htau BMD values were in range of female C57 and tau null values and were statistically indistinguishable. Dissimilar to their female counterparts, male htau BMD was consistently reduced from both male C57 and tau null mice for the 6–14 months duration of the homeostatic skeletal growth period (Fig. 2B; $p < 0.05$ in all monthly comparisons). Interestingly, male tau null BMD was significantly greater than their htau siblings but was indistinguishable from male C57, indicating that a low BMD skeletal phenotype was attributable to carrier status of the mutant human tau transgene. All mice in the study began showing an age-related decline in overall BMD around 11–14 months that was more pronounced among male mice (Fig. 2).

3.2. Htau mice exhibit large magnitude sex differences in overall skeletal BMD across the homeostatic remodeling phase

To directly analyze sex differences in BMD within each strain, an aggregate homeostatic BMD variable was created by averaging BMD values across the entire 6–14 month period. These average homeostatic BMD values are plotted in Fig. 2C. Males in both C57 ($F_{1,8}$ = 20.09, p =0.002) and htau ($F_{1,8}$ = 117.9, $p < 0.001$) strain groups demonstrated significantly lower BMD than their respective females. The magnitude of this sex difference in male htau far exceeded that of C57 males, with male htau experiencing a 9% lower reduction in bone mass from female htau mice compared to a 4% reduction inmale C57 bone mass compared to female C57s. No sex differences were shown among tau null mice ($F_{1,8} = 0.15$, p = ns).

3.3. Male htau mice exhibit reduced BMD at individual bones across the homeostatic remodeling phase

Average homeostatic BMD data for the femur and lumbar spine are plotted in Fig. 2D. Significant strain by sex interactions in femoral density were indicated by analyses ($F_{2,23} = 8.35$, $p = 0.002$). Female mice did not differ in femoral BMD, but male htau exhibited lower values than both C57 and tau null males ($F_{2,12}$ = 18.71,

$p < 0.001$) and lower femoral BMD compared to female htau ($F_{1,8} = 21.52$, $p = 0.002$). While C57 femur density did not differ by sex, male tau null mice had significantly denser femur than their females ($F_{1,8} = 6.1$, $p = 0.04$). Analyses of lumbar spine density also revealed a significant strain by sex interaction ($F_{2,23} = 6.0$, $p = 0.008$). Again, lumbar BMD did not differ among female mice of any strain, but among males, htau spine density was significantly lower than C57 mice ($F_{2,12} = 7.8$, $p = 0.001$) but not tau nulls. Male tau null lumbar BMD seemed to occupy values somewhere between C57 and htau, which failed to distinguish them from either of those groups (see Fig. 2D). No sex differences in lumbar BMD were indicated among C57 or tau null mice, but male htau had lower spine density than their females ($F_{1,8} = 26.51$, $p = 0.001$). Collectively, these findings show that phenotype alterations in male htau skeletal density are measurable across multiple bone sites.

3.4. Body mass and body fat composition are elevated in C57 control mice relative to other strains

Average body mass and fat composition across the homeostatic skeletal remodeling period are plotted in Fig. 3. Body mass differed by sex ($F_{1,23} = 12.49$, $p < 0.002$) and strain ($F_{2,23} = 16.4$, $p < 0.001$) with no significant interaction between these variables. Among females, C57 exhibited greater body mass than both htau (Bonferroni-adjusted $p = 0.04$) and tau nulls (Bonferroni-adjusted $p = 0.04$), $F_{2,11} = 5.71$, $p = 0.02$, an interesting distinction, given that BMD did not differ between C57 and these strains. Female htau and tau null body mass did not differ from each other. C57 males also weighed significantly more than both htau (Bonferroni-adjusted $p = 0.001$) and tau null males (Bonferroni-adjusted $p = 0.02$), $F_{2,11} = 5.1$, $p = 0.02$. Htau and tau null males did not differ from each other in body mass, despite displaying large differences in BMD (recall Fig. 2B). This finding indicates that body mass was not the driving factor for low BMD bone in male htau mice. Direct sex differences were not compared within each strain as it was anticipated that male mice would weigh more than female mice overall. In analyses of body fat composition, only significant strain differences were indicated ($F_{2,23} = 12.05$, $p < 0.001$), with C57 mice having elevated body fat composition compared to htau and tau null mice, $F_{2,27} = 14.04$, $p < 0.001$ (Bonferroni-adjusted $p = 0.001$ for each individual comparison).

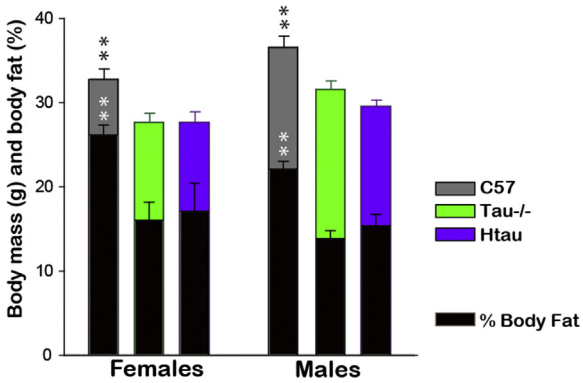

Fig. 3. Body mass and body fat composition averaged across the homeostatic remodeling period from 6–14 months of age. Stacked bars depict body mass (colored portion) and percent body fat (black portion) for female (left) and male (right) C57 (gray), tau −/− (green), and htau (purple) mice. Y-axis provides absolute (not relative) scale values for average grams of body mass and percent body fat. Female C57 mice weighed significantly more (black asterisks) and had greater percent body fat (white asterisks) than both tau −/− and htau females ($p < 0.05$). Htau and tau −/− do not differ on either variable. This exact pattern of findings was reflected among males. Error bars depict standard error of the mean.

3.5. Decreased expression of osteogenic genes indicates compromised skeletal health in male and female htau mice

Expression of osteogenic genes *Col1a1* and *Col5a1* can be used as an assessment of bone formation and strength as well as remodeling integrity (Chaplin et al., 2015; Wu et al., 2010), and expression levels measured from the tibia and femur of 14-month-old mice are presented in Fig. 4. Both *Col1a1* ($F_{2,29} = 22.69$, $p < 0.001$) and *Col5a1* ($F_{2,29} = 17.95$, $p < 0.001$) expression levels in bone differed by strain and were significantly reduced in both female and male htau bone compared to C57 and tau null samples (Bonferroni-adjusted $p < 0.001$ in all comparisons). *Col1a1* expression in male htau bone was further reduced from female htau, $F_{1,10} = 18.53$, $p = 0.002$, likely reflected the severity of the low BMD phenotype presentation in males. While *Col5a1* expression trended lower in male htau compared to their females, this effect was not significant. Male C57 mice had greater expression of these genes compared to female C57s, $F_{1,8} = 11.31$, $p = 0.01$. Collectively, these findings further support the impaired skeletal phenotype in male htau, but most importantly, provide a striking indication that female htau skeletal remodeling processes are also compromised, albeit in ways that were not detectible with radiographic densitometry.

3.6. Alterations in peripheral Wnt pathway gene expression are associated with skeletal compromise in htau mice

Assessment of specific Wnt genes was targeted to components of the canonical signaling pathway known to be associated with either osteoporosis or Alzheimer's-associated neuropathology (recall Table 1). Targeted genes represented multiple levels of signaling within the cellular Wnt/βcat pathway. Expression levels measured from the tibia and femur of 14-month-old mice are presented in Fig. 5. Significant alterations in gene expression measured in htau bones were identified for *CTNNB1* ($F_{2,29} = 99.47$, $p < 0.001$), *Dkk1* ($F_{2,29} = 43.36$, $p < 0.001$), *Sost* ($F_{2,29} = 87.89$, $p < 0.001$), *Lrp* ($F_{2,29} = 59.44$, $p < 0.001$), and *Runx2* ($F_{2,29} = 50.42$, $p < 0.001$). At the extracellular signaling level, htau bone exhibited significantly increased mRNA levels of *Dkk1*, a systemic Wnt antagonist and *Sost*, a Wnt antagonist expressed locally in bone cells compared to controls (Bonferroni-corrected $p < 0.001$ in all comparisons). However, there were no differences between strain groups in the expression of the endogenous Wnt activator *Wnt3a*, suggesting that increased inhibition of the Wnt/βcat pathway may be the initiator of Wnt dysfunction as opposed to deficient endogenous activation.

Decreased expression of Wnt co-receptor *Lrp5* gene was detected in htau bone compared to controls ($p < 0.001$). Consequently, htau bone showed a significant reduction in *βcat* expression compared to C57 and tau null bone ($p < 0.001$). *Runx2*, a transcription factor and regulator of osteoblast function that is activated by *βcat* at the nuclear level (Reinhold and Naski, 2007), was also significantly reduced in htau bone compared to controls ($p < 0.001$), with male htau showing significantly greater deficits than female htau ($F_{1,10} = 6.12$, $p = 0.03$). Collectively, these data indicate that multiple components of Wnt/βcat signaling are disrupted in htau bone compared to controls. This pattern is also consistent with those previously reported for accompanying osteoporotic bone loss triggered by Dkk1 or SOST antagonism of the Wnt pathway (Mao et al., 2002; Marsell et al., 2012).

3.7. Alterations in central Wnt pathway gene expression differentiate htau mice from controls

Data summarizing expression levels of Wnt/βcat genes for hippocampus and brainstem of 14-month-old mice are presented in Fig. 6. The same Wnt gene targets were assayed in brain tissue as in

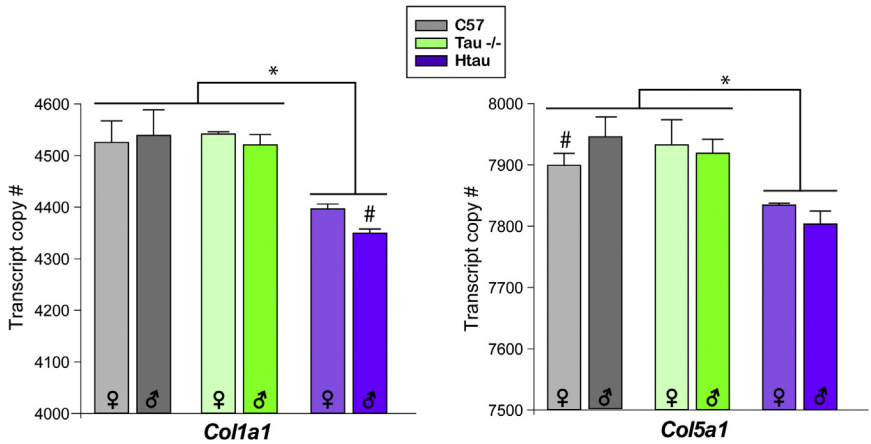

Fig. 4. Expression levels of osteogenic genes in bone samples taken from the tibia and femur of 14-month-old mice. Average transcript copy number (per 50 ng mRNA) is plotted for female (♀) and male (♂) mice of each strain as coded in legend. Expression levels of bone formation/strength indicators *Col1a1* and *Col5a1* are significantly reduced in htau mice (both sexes) relative to controls. Male htau mice showed further reduction in *Col1a1* expression from htau females. In C57 mice, male *Col5a1* expression was elevated compared to females. Asterisk indicates significant strain differences of ($p < 0.01$); # indicates significant sex differences of ($p < 0.01$); error bars depict standard error of the mean.

bone with the following substitutions: endogenous Wnt activator *Wnt7a*, which is involved regulating neuronal function, *Lrp6*, the form of Wnt coreceptor predominantly expressed in brain tissue, and *TCF4*, a DNA-binding protein that suppresses pathological protein processing in AD. In the hippocampus, a brain region where htau mice typically show tau pathology, htau mice expressed significantly reduced levels of *Lrp6* ($F_{2,19} = 16.82$, $p < 0.001$), *βcat* ($F_{2,19} = 7.9$, $p = 0.003$), and *TCF4* ($F_{2,12} = 4.6$, $p = 0.03$). Notably, *Dkk1* expression did not differ by strain group in this brain region. In the brainstem, a region involved in regulation of homeostatic bone remodeling and an area where tau pathology emerges very early on in htau mice, expression levels of *Wnt7a* ($F_{2,26} = 7.2$, $p = 0.003$) and *Lrp6* ($F_{2,26} = 4.94$ $p = 0.02$) were all significantly reduced in htau compared to both C57 and tau null controls ($p < 0.5$). Brainstem *TCF4* ($F_{2,25} = 4.94$, $p = 0.02$) expression trended toward a reduction in htau compared to controls, but this effect did not reach significance. Brainstem *Dkk1* expression differed by strain as a function of sex ($F_{2,19} = 4.05$, $p = 0.03$), with female htau demonstrating very high levels compared to both C57 ($p < 0.01$) and tau null females ($p = 0.02$). Male mice did not differ by strain in *Dkk1* expression. However, male mice registered significantly lower *Dkk1* gene expression than their female counterparts ($F_{1,8} = 16.51$, $p = 0.005$). Similar to gene expression results from bone, these data from htau brain tissue confirm alterations in Wnt gene expression patterns that indicate aged htau mice uniquely experience perturbations in Wnt signaling.

4. Discussion

Insufficient Wnt/βcat activation impairs bone remodeling (Krishnan et al., 2006) and contributes to AD pathogenesis (Tapia-Rojas et al., 2016), albeit in distinctly separate contexts. This study is the first to show altered gene expression related to Wnt/βcat signaling in a mouse model that exhibits both low BMD and AD-like tauopathy. These data show that htau mice sustain a compromised skeletal phenotype beyond 6 months of age and until at least

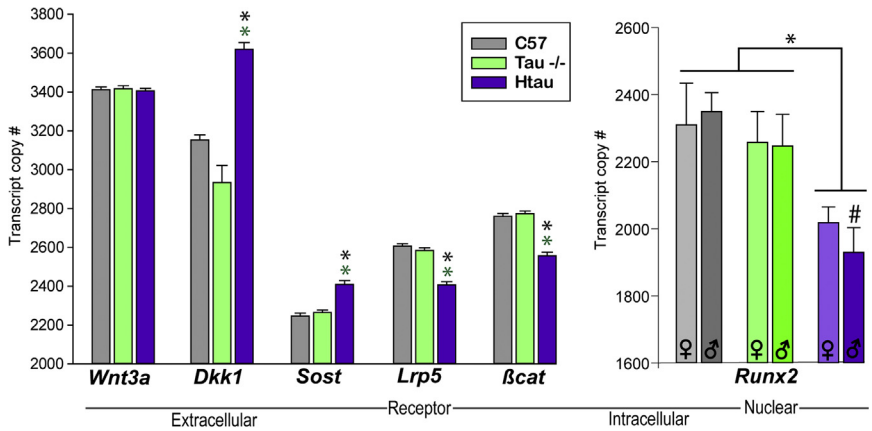

Fig. 5. Gene expression levels for select Wnt pathway components measured in the tibia and femur of 14-month-old mice. Average transcript copy number (per 50 ng mRNA) is plotted for genes associated with extracellular Wnt ligands (*Wnt3a*) and antagonists (*Dkk1* and *Sost*), coreceptor *Lrp5*, intracellular signaling molecule beta catenin (βcat; *CTNNB1β*), and nuclear transcription factor *Runx2*. Expression data for most genes did not differ by sex and are collapsed across this variable in the first graph; sex differences were indicated for *Runx2* which is plotted separately. Strain groups are coded in legend. No differences in *Wnt3a* expression were shown by strain; *Dkk1* and *Sost* mRNA levels were increased in htau bone compared to controls. Expression of the Wnt coreceptor *Lrp5* gene was reduced in htau bone, with a corresponding reduction in *βcat*. At the nuclear level, transcription factor and promoter of bone formation *Run2x* was also reduced in htau mice compared to controls, with male (♂) htau bone exhibiting further deficiency in *Runx2* mRNA compared to their female (♀) counterparts. Lines and labels at bottom of figure categorize Wnt components by the cellular level at which they signal in the pathway. Green asterisks indicate significant differences between htau and tau −/−; back asterisks indicate significant differences between htau and C57 (both at $p < 0.01$). # indicates significant differences between sexes ($p < 0.01$). Error bars depict standard error of the mean.

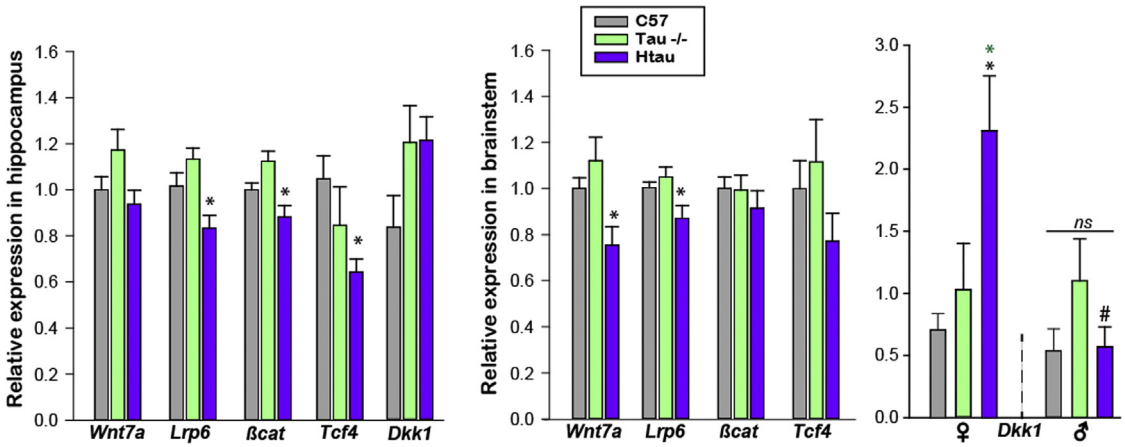

Fig. 6. Expression levels of Wnt pathway genes measured in the hippocampus (left) and brainstem (right) of 14-month-old mice. Relative expression (fold change) from calibration control is plotted for each gene across strains. Coding for strains is shown in legend. Htau hippocampus showed significant reductions in expression compared to controls for the following genes: *Lrp6*, *βcat*, and *Tcf4*. Hippocampal expression of Wnt antagonist *Dkk1* did not differ by strain. In the brainstem, htau mice had reduced expression of *Wnt7a and Lrp6*, and nonsignificant trend toward reduced *Tcf4* levels compared to controls. Htau brainstem expression of *Dkk1* exhibited sex differences and is shown on separate plot (note difference in y-axis scale). Female htau brainstem expression of *Dkk1* was significantly elevated from female C57 and tau −/− controls. Black asterisks indicate significant difference from C57; green asterisk indicates significant difference from tau nulls ($p < 0.05$). While male mice did not differ in brainstem *Dkk1* expression, male htau exhibited significantly lower expression than female htau ($p < 0.01$). ♀ indicates data for female mice; ♂ indicates data for males.

14 months, with the severity and manner of low bone mass presentation differing by sex. Male htau mice experienced a profound reduction in bone mass, measured using radiographic densitometry, from as early as 3 months, persisting until 14 months. In contrast, female htau mice demonstrated an early low BMD phenotype during the period of anabolic skeleton growth from 3 to 6 months of age but then attain what appears to be normal bone mass around the time they enter the adult homeostatic skeletal remodeling period (7 months). However, at 14 months, female htau mice exhibited strong indication of impairment in skeletal remodeling processes as evidenced by reduced osteogenic and Wnt pathway gene expression in bone. It is possible female bone changes in more subtle ways or that the bone-enhancing effects of circulating estrogens (Yang et al., 2013) compensate for changes in remodeling processes. These questions may need to be addressed in future studies tracking microarchitectural changes in bone tissue composition as a function of reproductive status.

Bone loss and AD-associated pathology have been linked with dysfunction at multiple levels of signaling in the Wnt/βcat pathway (Inestrosa and Varela-Nallar, 2014; Liu et al., 2014; Parr et al., 2015; Riise et al., 2015; Scali et al., 2006). In the present study, htau bone exhibited increased expression of *Dkk1* and *Sost* (sclerostin), which encode for proteins that antagonize the Wnt/βcat pathway at initial stages of signaling. Both Dkk1 and sclerostin have been associated with reduction in bone formation/quality (Glantschnig et al., 2011; Pérez-Campo et al., 2016). Dkk1 plays several roles in AD pathogenesis (Caricasole et al., 2004). It is overactivated by the pathological protein Aβ (Purro et al., 2012), causing Wnt suppression and triggering a series of downstream effects that promote hyperphosphorylation of tau (Salcedo-Tello et al., 2014) and promote cleavage of additional toxic Aβ fragments, further perpetuating Wnt dysfunction and pathological protein accumulation. Although problematic as described in the preceding scenario, Wnt antagonists represent a potential target for therapeutic intervention. Pharmacological agents that reduce Dkk1 overexpression could benefit bone health (Glantschnig et al., 2011) and potentially slow neurodegeneration (Caraci et al., 2008). Anti-sclerostin therapies are currently being tested as therapeutics in osteoporosis and may present a viable treatment option for bone fragility in AD (Recker et al., 2015).

In htau brain, but not bone, our data suggest impairment in endogenous Wnt ligand activation, as we detected reductions in *Wnt7a* in multiple brain regions. Again, this finding supports the potential to target Wnt activators therapeutically to resolve Wnt signaling deficiencies in disease. Both endogenous and synthetic Wnt agonists have shown neuroprotective potential in mouse models of AD, reducing ptau and Aβ load, and restoring synaptic function that was previously perturbed by such pathology (Chacón et al., 2008; Vargas et al., 2015).

Across both the bone and brain, we observed reductions in expression of Wnt coreceptor *LRP5/6*. Dkk1 and SOST exert their antagonist action by binding to these receptors, with Dkk1 triggering the protein Kremin to endocytose LRP5/6 (Mao and Niehrs, 2003), preventing βcat activation (Riise et al., 2015). Genetic variants in *LRP6* associated with deficient Wnt/βcat signaling are linked to increased late-onset AD risk (Alarcón et al., 2013; De Ferrari et al., 2007). Notably, apolipoprotein E, of which the inherited variant apolipoprotein E-ε4 allele predisposes risk for AD (Corder et al., 1993), signals through the LRP family of proteins (De Ferrari et al., 2007). Loss of function in this receptor has been shown to enhance Aβ pathology, inflammation, and synapse loss (Liu et al., 2014). Since LRP5/6 activation normally inhibits glycogen synthase kinase 3β (recall Fig. 1), loss of LRP function enables this kinase to phosphorylate both βcat and tau, suppressing activity of the former and causing pathological changes in the latter (Salcedo-Tello et al., 2014; Scali et al., 2006). Glycogen synthase kinase 3β is one of the principle kinases involved in tau hyperphosphorylation that causes ptau to dissociate from axonal microtubules and aggregate into neurofibrillary tangles that contribute to neurodegeneration (Aamodt and Williams, 1984; Braak and Braak, 1991).

Dysfunction of the canonical Wnt cascade at critical intracellular signaling levels was also indicated in both htau bone and brain tissue with significantly reduced expression of *βcat*. Other studies observed reduced levels of this major transcriptional coactivator in postmortem AD patient brains (Toledo and Inestrosa, 2010), an observation that has also been linked with the *presenilin-1* mutation that confers susceptibility to the early-onset familial form of AD (Zhang et al., 1998). As a likely sequelae of βcat reduction in htau mice, we observed reduced expression

of transcription factors *Runx2* and *Tcf4*. In bone, RUNX2 acts as major regulator of bone formation, activating a number of downstream targets that facilitate positive skeletal remodeling processes (Pérez-Campo et al., 2016). In brain, DNA-binding protein TCF4 has been identified as having a neuroprotective role, with evidence that it suppresses production of both ptau and Aβ (Parr et al., 2015; Tapia-Rojas et al., 2016). Extracellular Aβ plaques consist of neurotoxic fragments that are cleaved from APP by beta secretase cleavage enzyme 1 (BACE1; Yan et al., 1999). TCF4 can powerfully suppress the *Bace1* promotor (Parr et al., 2015), limiting BACE1 activity. However, Wnt/βcat inhibition prevents this, and BACE1 activity can go unchecked (Tapia-Rojas et al., 2016). Collectively, these findings support the idea that impairments in canonical Wnt signaling occur in both bone and brain tissue of htau mice, suggesting that vulnerabilities in this molecular cascade may contribute to itsskeletal and neuropathological phenotype. This opens up a number of research questions, particularly with regard to the time course of Wnt signaling alterations in this model. In early or presymptomatic disease states, is Wnt signaling selectively vulnerable to pathophysiological processes of AD, or, does a predisposition toward deficient Wnt signaling enable AD pathology to take hold? Answers to these questions are currently being pursued by members of our research team.

5. Conclusions

Overall, the data from this study provoke a number of new questions about common signaling pathway dysfunction across multiple organ systems in AD, and promote an ideological shift from viewing this disease as relegated to the nervous system to one that affects multiple tissues. AD is vastly complex and likely encompasses multiple etiologies and presentations—with or without comorbid bone loss. Therefore, the results of the present study may only be generalizable to variants of the disease characterized by this comorbidity. However, this variant is worthy of attention, given its prevalence and the profound impact skeletal fracture has on quality of life in AD patients. Low BMD may indicate a particular disease etiology that is triggered or exacerbated by underlying Wnt signaling deficiencies. Identification of such factors may provide opportunities to use personalized/precision medicine approaches to treat individuals most likely to benefit from therapeutic modification of Wnt/βcat signaling (Cholerton et al., 2016; Hampel et al., 2017). The potential advantages range from improving quality of life by correcting bone loss to slowing the progression of a neurodegenerative mechanism.

Disclosure statement

The authors have no actual or potential conflicts of interest.

Acknowledgements

Mr. Urmil Patel is thanked for assistance with molecular data collection. Adam Schuller, Jon Meier, and Suzie Abdeljalil are thanked for their help with tissue collection. The authors are grateful to Dr. Matthew A. Smith and Dr. Samuel D. Crish for their assistance in editing this article. The authors would like to thank Ms. Ellie Kleber for proofreading the article.

This work was supported by the National Science Foundation (NSF-CMMI1537745 to LNC) and by institutional research start-up funds (Northeast Ohio Medical University to CMD-C).

Appendix A. Supplementary data

Supplementary data associated with this article can be found, in the online version, at https://doi.org/10.1016/j.neurobiolaging.2018.03.021.

References

Aamodt, E.J., Williams, R.C., 1984. Microtubule-associated proteins connect microtubules and neurofilaments in vitro. Biochemistry 23, 6023–6031.
Aberle, H., Bauer, A., Stappert, J., Kispert, A., Kemler, R., 1997. beta-catenin is a target for the ubiquitin-proteasome pathway. EMBO J. 16, 3797–3804.
Alarcón, M.A., Medina, M.A., Hu, Q., Avila, M.E., Bustos, B.I., Pérez-Palma, E., Peralta, A., Salazar, P., Ugarte, G.D., Reyes, A.E., Martin, G.M., Opazo, C., Moon, R.T., De Ferrari, G.V., 2013. A novel functional low-density lipoprotein receptor-related protein 6 gene alternative splice variant is associated with Alzheimer's disease. Neurobiol. Aging 34, 1709.e9-1709.e18.
Amouzougan, A., Lafaie, L., Marotte, H., Dénarié, D., Collet, P., Pallot-Prades, B., Thomas, T., 2017. High prevalence of dementia in women with osteoporosis. Joint Bone Spine 84, 611–614.
Andorfer, C., Kress, Y., Espinoza, M., de Silva, R., Tucker, K.L., Barde, Y.-A., Duff, K., Davies, P., 2003. Hyperphosphorylation and aggregation of tau in mice expressing normal human tau isoforms. J. Neurochem. 86, 582–590.
Arce, L., Yokoyama, N.N., Waterman, M.L., 2006. Diversity of LEF/TCF action in development and disease. Oncogene 25, 7492–7504.
Ball, H.C., Holmes, R.K., Londraville, R.L., Thewissen, J.G.M., Duff, R.J., 2013. Leptin in Whales: validation and measurement of mRNA expression by absolute quantitative real-time PCR. PLoS One 8, e54277.
Ball, H.C., Moussa, F.M., Mbimba, T., Orman, R., Safadi, F.F., Cooper, L.N., 2016. Methods and insights from the characterization of osteoprogenitor cells of bats (Mammalia: Chiroptera). Stem Cell Res. 17, 54–61.
Beamer, W.G., Donahue, L.R., Rosen, C.J., Baylink, D.J., 1996. Genetic variability in adult bone density among inbred strains of mice. Bone 18, 397–403.
Bemiller, S.M., McCray, T.J., Allan, K., Formica, S.V., Xu, G., Wilson, G., Kokiko-Cochran, O.N., Crish, S.D., Lasagna-Reeves, C.A., Ransohoff, R.M., Landreth, G.E., Lamb, B.T., 2017. TREM2 deficiency exacerbates tau pathology through dysregulated kinase signaling in a mouse model of tauopathy. Mol. Neurodegener 12, 74.
Bennett, C.N., Longo, K.A., Wright, W.S., Suva, L.J., Lane, T.F., Hankenson, K.D., MacDougald, O.A., 2005. Regulation of osteoblastogenesis and bone mass by Wnt10b. Proc. Natl. Acad. Sci. U. S. A. 102, 3324–3329.
Bonafede, M., Shi, N., Barron, R., Li, X., Crittenden, D.B., Chandler, D., 2016. Predicting imminent risk for fracture in patients aged 50 or older with osteoporosis using US claims data. Arch. Osteoporos. 11, 26.
Bourhis, E., Wang, W., Tam, C., Hwang, J., Zhang, Y., Spittler, D., Huang, O.W., Gong, Y., Estevez, A., Zilberleyb, I., Rouge, L., Chiu, C., Wu, Y., Costa, M., Hannoush, R.N., Franke, Y., Cochran, A.G., 2011. Wnt antagonists bind through a short peptide to the first β-propeller domain of LRP5/6. Structure 19, 1433–1442.
Braak, H., Braak, E., 1991. Neuropathological stageing of Alzheimer-related changes. Acta Neuropathol. 82, 239–259.
Bustin, S.A., 2002. Quantification of mRNA using real-time reverse transcription PCR (RT-PCR): trends and problems. J. Mol. Endocrinol. 29, 23–39.
Caraci, F., Busceti, C., Biagioni, F., Aronica, E., Mastroiacovo, F., Cappuccio, I., Battaglia, G., Bruno, V., Caricasole, A., Copani, A., Nicoletti, F., 2008. The Wnt antagonist, Dickkopf-1, as a target for the treatment of neurodegenerative disorders. Neurochem. Res. 33, 2401–2406.
Caricasole, A., Copani, A., Caraci, F., Aronica, E., Rozemuller, A.J., Caruso, A., Storto, M., Gaviraghi, G., Terstappen, G.C., Nicoletti, F., 2004. Induction of Dickkopf-1, a negative modulator of the Wnt pathway, is associated with neuronal degeneration in Alzheimer's brain. J. Neurosci. 24, 6021–6027.
Chacón, M.A., Varela-Nallar, L., Inestrosa, N.C., 2008. Frizzled-1 is involved in the neuroprotective effect of Wnt3a against Aβ oligomers. J. Cell. Physiol 217, 215–227.
Chang, K.-H., Chung, C.-J., Lin, C.-L., Sung, F.-C., Wu, T.-N., Kao, C.-H., 2014. Increased risk of dementia in patients with osteoporosis: a population-based retrospective cohort analysis. Age (Omaha) 36, 967–975.
Chaplin, A., Palou, A., Serra, F., 2015. Body fat loss induced by calcium in co-supplementation with conjugated linoleic acid is associated with increased expression of bone formation genes in adult mice. J. Nutr. Biochem. 26, 1540–1546.
Cholerton, B., Larson, E.B., Quinn, J.F., Zabetian, C.P., Mata, I.F., Keene, C.D., Flanagan, M., Crane, P.K., Grabowski, T.J., Montine, K.S., Montine, T.J., 2016. Precision medicine. Am. J. Pathol. 186, 500–506.
Clevers, H., Nusse, R., 2012. Wnt/β-Catenin signaling and disease. Cell 149, 1192–1205.
Corder, E.H., Saunders, A.M., Strittmatter, W.J., Schmechel, D.E., Gaskell, P.C., Small, G.W., Roses, A.D., Haines, J.L., Pericak-Vance, M.A., 1993. Gene dose of apolipoprotein E type 4 allele and the risk of Alzheimer's disease in late onset families. Science 261, 921–923.
Cui, S., Xiong, F., Hong, Y., Jung, J.-U., Li, X.-S., Liu, J.-Z., Yan, R., Mei, L., Feng, X., Xiong, W.-C., 2011. APPswe/Aβ regulation of osteoclast activation and RAGE expression in an age-dependent manner. J. Bone Miner. Res. 26, 1084–1098.

De Ferrari, G.V., Papassotiropoulos, A., Biechele, T., Wavrant De-Vrieze, F., Avila, M.E., Major, M.B., Myers, A., Sáez, K., Henríquez, J.P., Zhao, A., Wollmer, M.A., Nitsch, R.M., Hock, C., Morris, C.M., Hardy, J., Moon, R.T., 2007. Common genetic variation within the low-density lipoprotein receptor-related protein 6 and late-onset Alzheimer's disease. Proc. Natl. Acad. Sci. U. S. A. 104, 9434–9439.

Dengler-Crish, C.M., Smith, M.A., Wilson, G.N., 2017. Early evidence of low bone density and decreased serotonergic synthesis in the dorsal raphe of a tauopathy model of Alzheimer's disease. J. Alzheimer's Dis. 55, 1605–1619.

Fernandes, J.M.O., Mommens, M., Hagen, Ø., Babiak, I., Solberg, C., 2008. Selection of suitable reference genes for real-time PCR studies of Atlantic halibut development. Comp. Biochem. Physiol. B Biochem. Mol. Biol. 150, 23–32.

Fuchs, H., Gau, C., Hans, W., Gailus-Durner, V., Hrabě de Angelis, M., 2013. Long-term experiment to study the development, interaction, and influencing factors of DEXA parameters. Mamm. Genome 24, 376–388.

Gargiulo, S., Gramanzini, M., Megna, R., Greco, A., Albanese, S., Manfredi, C., Brunetti, A., 2014. Evaluation of growth patterns and body composition in c57bl/6j mice using dual energy x-ray absorptiometry. Biomed. Res. Int. 2014, 253067.

Geiszler, P.C., Barron, M.R., Pardon, M.-C., 2016. Impaired burrowing is the most prominent behavioral deficit of aging htau mice. Neuroscience 329, 98–111.

Glantschnig, H., Scott, K., Hampton, R., Wei, N., McCracken, P., Nantermet, P., Zhao, J.Z., Vitelli, S., Huang, L., Haytko, P., Lu, P., Fisher, J.E., Sandhu, P., Cook, J., Williams, D., Strohl, W., Flores, O., Kimmel, D., Wang, F., An, Z., 2011. A rate-limiting role for Dickkopf-1 in bone formation and the remediation of bone loss in mouse and primate models of postmenopausal osteoporosis by an experimental therapeutic antibody. J. Pharmacol. Exp. Ther. 338, 568–578.

Guerreiro, R., Wojtas, A., Bras, J., Carrasquillo, M., Rogaeva, E., Majounie, E., Cruchaga, C., Sassi, C., Kauwe, J.S.K., Younkin, S., Hazrati, L., Collinge, J., Pocock, J., Lashley, T., Williams, J., Lambert, J.-C., Amouyel, P., Goate, A., Rademakers, R., Morgan, K., Powell, J., St George-Hyslop, P., Singleton, A., Hardy, J. Alzheimer Genetic Analysis Group, 2013. TREM2 variants in Alzheimer's disease. N. Engl. J. Med. 368, 117–127.

Hampel, H., O'Bryant, S.E., Durrleman, S., Younesi, E., Rojkova, K., Escott-Price, V., Corvol, J.-C., Broich, K., Dubois, B., Lista, S. Alzheimer Precision Medicine Initiative, 2017. A Precision Medicine Initiative for Alzheimer's disease: the road ahead to biomarker-guided integrative disease modeling. Climacteric 20, 107–118.

Inestrosa, N.C., Varela-Nallar, L., 2014. Wnt signaling in the nervous system and in Alzheimer's disease. J. Mol. Cell Biol. 6, 64–74.

Jay, T.R., Miller, C.M., Cheng, P.J., Graham, L.C., Bemiller, S., Broihier, M.L., Xu, G., Margevicius, D., Karlo, J.C., Sousa, G.L., Cotleur, A.C., Butovsky, O., Bekris, L., Staugaitis, S.M., Leverenz, J.B., Pimplikar, S.W., Landreth, G.E., Howell, G.R., Ransohoff, R.M., Lamb, B.T., 2015. TREM2 deficiency eliminates TREM2+ inflammatory macrophages and ameliorates pathology in Alzheimer's disease mouse models. J. Exp. Med. 212, 287–295.

Johansson, C., Skoog, I., 1996. A population-based study on the association between dementia and hip fractures in 85-year olds. Aging (Milano) 8, 189–196.

Jonsson, T., Stefansson, H., Steinberg, S., Jonsdottir, I., Jonsson, P.V., Snaedal, J., Bjornsson, S., Huttenlocher, J., Levey, A.I., Lah, J.J., Rujescu, D., Hampel, H., Giegling, I., Andreassen, O.A., Engedal, K., Ulstein, I., Djurovic, S., Ibrahim-Verbaas, C., Hofman, A., Ikram, M.A., van Duijn, C.M., Thorsteinsdottir, U., Kong, A., Stefansson, K., 2013. Variant of *TREM2* associated with the risk of Alzheimer's disease. N. Engl. J. Med. 368, 107–116.

Kajimura, D., Lee, H.W., Riley, K.J., Arteaga-Solis, E., Ferron, M., Zhou, B., Clarke, C.J., Hannun, Y.A., Depinho, R.A., Guo, E.X., Mann, J.J., Karsenty, G., 2013. Adiponectin regulates bone mass via opposite central and peripheral mechanisms through foxo1. Cell Metab 17, 901–915.

Komori, T., 2010. Regulation of osteoblast differentiation by Runx2. Adv. Exp. Med. Biol. 658, 43–49.

Komuro, Y., Xu, G., Bhaskar, K., Lamb, B.T., 2015. Human tau expression reduces adult neurogenesis in a mouse model of tauopathy. Neurobiol. Aging 36, 2034–2042.

Korvala, J., Jüppner, H., Mäkitie, O., Sochett, E., Schnabel, D., Mora, S., Bartels, C.F., Warman, M.L., Deraska, D., Cole, W.G., Hartikka, H., Ala-Kokko, L., Männikkö, M., 2012. Mutations in LRP5 cause primary osteoporosis without features of OI by reducing Wnt signaling activity. BMC Med. Genet. 13, 26.

Krishnan, V., Bryant, H.U., Macdougald, O.A., 2006. Regulation of bone mass by Wnt signaling. J. Clin. Invest 116, 1202–1209.

Liu, C., Li, Y., Semenov, M., Han, C., Baeg, G.H., Tan, Y., Zhang, Z., Lin, X., He, X., 2002. Control of beta-catenin phosphorylation/degradation by a dual-kinase mechanism. Cell 108, 837–847.

Liu, C.-C., Tsai, C.-W., Deak, F., Rogers, J., Penuliar, M., Sung, Y.M., Maher, J.N., Fu, Y., Li, X., Xu, H., Estus, S., Hoe, H.-S., Fryer, J.D., Kanekiyo, T., Bu, G., 2014. Deficiency in LRP6-mediated Wnt signaling contributes to synaptic abnormalities and amyloid pathology in Alzheimer's disease. Neuron 84, 63–77.

Looker, A.C., Borrud, L.G., Dawson-Hughes, B., Shepherd, J.A., Wright, N.C., 2012. Osteoporosis or low bone mass at the femur neck or lumbar spine in older adults: United States, 2005-2008. NCHS Data Brief 1–8.

Loskutova, N., Honea, R.A., Vidoni, E.D., Brooks, W.M., Burns, J.M., 2009. Bone density and brain atrophy in early Alzheimer's disease. J. Alzheimers. Dis. 18, 777–785.

Mao, B., Niehrs, C., 2003. Kremen2 modulates Dickkopf2 activity during Wnt/LRP6 signaling. Gene 302, 179–183.

Mao, J., Wang, J., Liu, B., Pan, W., Farr, G.H., Flynn, C., Yuan, H., Takada, S., Kimelman, D., Li, L., Wu, D., 2001. Low-density lipoprotein receptor-related protein-5 binds to Axin and regulates the canonical Wnt signaling pathway. Mol. Cell 7, 801–809.

Mao, B., Wu, W., Davidson, G., Marhold, J., Li, M., Mechler, B.M., Delius, H., Hoppe, D., Stannek, P., Walter, C., Glinka, A., Niehrs, C., 2002. Kremen proteins are Dickkopf receptors that regulate Wnt/β-catenin signalling. Nature 417, 664–667.

Marsell, R., Sisask, G., Nilsson, Y., Sundgren-Andersson, A.K., Andersson, U., Larsson, S., Nilsson, O., Ljunggren, O., Jonsson, K.B., 2012. GSK-3 inhibition by an orally active small molecule increases bone mass in rats. Bone 50, 619–627.

Melton, L.J., Beard, C.M., Kokmen, E., Atkinson, E.J., O'Fallon, W.M., 1994. Fracture risk in patients with Alzheimer's disease. J. Am. Geriatr. Soc. 42, 614–619.

Oliva, C.A., Vargas, J.Y., Inestrosa, N.C., 2013. Wnts in adult brain: from synaptic plasticity to cognitive deficiencies. Front. Cell. Neurosci 7, 224.

Otero, K., Shinohara, M., Zhao, H., Cella, M., Gilfillan, S., Colucci, A., Faccio, R., Ross, F.P., Teitelbaum, S.L., Takayanagi, H., Colonna, M., 2012. TREM2 and β-catenin regulate bone homeostasis by controlling the rate of osteoclastogenesis. J. Immunol. 188, 2612–2621.

Oury, F., Yadav, V.K., Wang, Y., Zhou, B., Liu, X.S., Guo, X.E., Tecott, L.H., Schutz, G., Means, A.R., Karsenty, G., 2010. CREB mediates brain serotonin regulation of bone mass through its expression in ventromedial hypothalamic neurons. Genes Dev. 24, 2330–2342.

Paloneva, J., Kestilä, M., Wu, J., Salminen, A., Böhling, T., Ruotsalainen, V., Hakola, P., Bakker, A.B., Phillips, J.H., Pekkarinen, P., Lanier, L.L., Timonen, T., Peltonen, L., 2000. Loss-of-function mutations in TYROBP (DAP12) result in a presenile dementia with bone cysts. Nat. Genet. 25, 357–361.

Panda, D., Samuel, J.C., Massie, M., Feinstein, S.C., Wilson, L., 2003. Differential regulation of microtubule dynamics by three- and four-repeat tau: implications for the onset of neurodegenerative disease. Proc. Natl. Acad. Sci. U. S. A. 100, 9548–9553.

Parr, C., Mirzaei, N., Christian, M., Sastre, M., 2015. Activation of the Wnt/β-catenin pathway represses the transcription of the β-amyloid precursor protein cleaving enzyme (BACE1) via binding of T-cell factor-4 to BACE1 promoter. FASEB J. 29, 623–635.

Peng, Y., Liu, J., Tang, Y., Liu, J., Han, T., Han, S., Li, H., Hou, C., Liu, J., Long, J., 2014. High-fat-diet-Induced weight gain ameliorates bone loss without exacerbating AβPP processing and cognition in female APP/PS1 mice. Front. Cell. Neurosci 8, 225.

Pérez-Campo, F.M., Santurtún, A., García-Ibarbia, C., Pascual, M.A., Valero, C., Garcés, C., Sañudo, C., Zarrabeitia, M.T., Riancho, J.A., 2016. Osterix and RUNX2 are transcriptional regulators of sclerostin in human bone. Calcif. Tissue Int. 99, 302–309.

Polydoro, M., Acker, C.M., Duff, K., Castillo, P.E., Davies, P., 2009. Age-dependent impairment of cognitive and synaptic function in the htau mouse model of tau pathology. J. Neurosci. 29, 10741–10749.

Purro, S.A., Dickins, E.M., Salinas, P.C., 2012. The secreted Wnt antagonist Dickkopf-1 is required for amyloid β-mediated synaptic loss. J. Neurosci. 32, 3492–3498.

Recker, R.R., Benson, C.T., Matsumoto, T., Bolognese, M.A., Robins, D.A., Alam, J., Chiang, A.Y., Hu, L., Krege, J.H., Sowa, H., Mitlak, B.H., Myers, S.L., 2015. A randomized, double-blind phase 2 clinical trial of blosozumab, a sclerostin antibody, in postmenopausal women with low bone mineral density. J. Bone Miner. Res. 30, 216–224.

Reinhold, M.I., Naski, M.C., 2007. Direct interactions of Runx2 and canonical Wnt signaling induce FGF18. J. Biol. Chem. 282, 3653–3663.

Riise, J., Plath, N., Pakkenberg, B., Parachikova, A., 2015. Aberrant Wnt signaling pathway in medial temporal lobe structures of Alzheimer's disease. J. Neural Transm. 122, 1303–1318.

Ross, R.D., Shah, R.C., Leurgans, S., Bottiglieri, T., Wilson, R.S., Sumner, D.R., 2018. Circulating Dkk1 and TRAIL are associated with cognitive decline in community-dwelling, older adults with cognitive concerns. J. Gerontol. A Biol. Sci. Med. Sci. https://doi.org/10.1093/gerona/glx252 [Epub ahead of print].

Salcedo-Tello, P., Hernández-Ortega, K., Arias, C., 2014. Susceptibility to GSK3β-induced tau phosphorylation differs between the young and aged hippocampus after Wnt signaling inhibition. J. Alzheimers. Dis. 39, 775–785.

Scali, C., Caraci, F., Gianfriddo, M., Diodato, E., Roncarati, R., Pollio, G., Gaviraghi, G., Copani, A., Nicoletti, F., Terstappen, G.C., Caricasole, A., 2006. Inhibition of Wnt signaling, modulation of Tau phosphorylation and induction of neuronal cell death by DKK1. Neurobiol. Dis. 24, 254–265.

Shi, Y., Oury, F., Yadav, V.K., Wess, J., Liu, X.S., Guo, X.E., Murshed, M., Karsenty, G., 2010. Signaling through the M3 muscarinic receptor favors bone mass accrual by decreasing sympathetic activity. Cell Metab 11, 231–238.

Sohrabi, H.R., Bates, K.A., Weinborn, M., Bucks, R.S., Rainey-Smith, S.R., Rodrigues, M.A., Bird, S.M., Brown, B.M., Beilby, J., Howard, M., Criddle, A., Wraith, M., Taddei, K., Martins, G., Paton, A., Shah, T., Dhaliwal, S.S., Mehta, P.D., Foster, J.K., Martins, I.J., Lautenschlager, N.T., Mastaglia, F., Laws, S.M., Martins, R.N., 2015. Bone mineral density, adiposity, and cognitive functions. Front. Aging Neurosci. 7, 1–10.

Tamimi, I., Ojea, T., Sanchez-Siles, J.M., Rojas, F., Martin, I., Gormaz, I., Perez, A., Dawid-Milner, M.S., Mendez, L., Tamimi, F., 2012. Acetylcholinesterase inhibitors and the risk of hip fracture in Alzheimer's disease patients: a case-control study. J. Bone Miner. Res. 27, 1518–1527.

Tan, Z.S., Seshadri, S., Beiser, A., Zhang, Y., Felson, D., Hannan, M.T., Au, R., Wolf, P.A., Kiel, D.P., 2005. Bone mineral density and the risk of Alzheimer disease. Arch. Neurol. 62, 107–111.

Tapia-Rojas, C., Burgos, P.V., Inestrosa, N.C., 2016. Inhibition of Wnt signaling induces amyloidogenic processing of amyloid precursor protein and the production and aggregation of Amyloid-β (Aβ) $_{42}$ peptides. J. Neurochem. 139, 1175–1191.

Toledo, E.M., Inestrosa, N.C., 2010. Activation of Wnt signaling by lithium and rosiglitazone reduced spatial memory impairment and neurodegeneration in brains of an APPswe/PSEN1DeltaE9 mouse model of Alzheimer's disease. Mol. Psychiatry 15, 272–285, 228.

Vargas, J.Y., Ahumada, J., Arrázola, M.S., Fuenzalida, M., Inestrosa, N.C., 2015. WASP-1, a canonical Wnt signaling potentiator, rescues hippocampal synaptic impairments induced by Aβ oligomers. Exp. Neurol. 264, 14–25.

Warner, R., 2013. Applied Statistics: From Bivariate through Multivariate Techniques, second ed. SAGE Publications, Thousand Oaks, CA.

Watanabe, K., Hishiya, A., 2005. Mouse models of senile osteoporosis. Mol. Aspects Med. 26, 221–231.

Weller, I., Schatzker, J., 2004. Hip fractures and Alzheimer's disease in elderly institutionalized Canadians. Ann. Epidemiol. 14, 319–324.

Westendorf, J.J., Kahler, R.A., Schroeder, T.M., 2004. Wnt signaling in osteoblasts and bone diseases. Gene 341, 19–39.

Willert, K., Shibamoto, S., Nusse, R., 1999. Wnt-induced dephosphorylation of axin releases beta-catenin from the axin complex. Genes Dev. 13, 1768–1773.

Wu, Y.-F., Matsuo, N., Sumiyoshi, H., Yoshioka, H., 2010. Sp7/Osterix is involved in the up-regulation of the mouse pro-α1(V) collagen gene (Col5a1) in osteoblastic cells. Matrix Biol. 29, 701–706.

Xia, W.-F., Jung, J.-U., Shun, C., Xiong, S., Xiong, L., Shi, X.-M., Mei, L., Xiong, W.-C., 2013. Swedish mutant APP suppresses osteoblast differentiation and causes osteoporotic deficit, which are ameliorated by N-acetyl-L-cysteine. J. Bone Miner. Res. 28, 2122–2135.

Yadav, V.K., Oury, F., Suda, N., Liu, Z.-W., Gao, X.-B., Confavreux, C., Klemenhagen, K.C., Tanaka, K.F., Gingrich, J.A., Guo, X.E., Tecott, L.H., Mann, J.J., Hen, R., Horvath, T.L., Karsenty, G., 2009. A serotonin-dependent mechanism explains the leptin regulation of bone mass, appetite, and energy expenditure. Cell 138, 976–989.

Yan, R., Bienkowski, M.J., Shuck, M.E., Miao, H., Tory, M.C., Pauley, A.M., Brashier, J.R., Stratman, N.C., Mathews, W.R., Buhl, A.E., Carter, D.B., Tomasselli, A.G., Parodi, L.A., Heinrikson, R.L., Gurney, M.E., 1999. Membrane-anchored aspartyl protease with Alzheimer's disease beta-secretase activity. Nature 402, 533–537.

Yang, M.W., Wang, T.H., Yan, P.P., Chu, L.W., Yu, J., Gao, Z.D., Li, Y.Z., Guo, B.L., 2011. Curcumin improves bone microarchitecture and enhances mineral density in APP/PS1 transgenic mice. Phytomedicine 18, 205–213.

Yang, Y.-H., Chen, K., Li, B., Chen, J.-W., Zheng, X.-F., Wang, Y.-R., Jiang, S.-D., Jiang, L.-S., 2013. Estradiol inhibits osteoblast apoptosis via promotion of autophagy through the ER–ERK–mTOR pathway. Apoptosis 18, 1363–1375.

Yuan, J.S., Burris, J., Stewart, N.R., Mentewab, A., Stewart, C.N., 2007. Statistical tools for transgene copy number estimation based on real-time PCR. BMC Bioinformatics 8 Suppl 7, S6.

Zhang, Z., Hartmann, H., Minh Do, V., Abramowski, D., Sturchler-Pierrat, C., Staufenbiel, M., Sommer, B., van de Wetering, M., Clevers, H., Saftig, P., De Strooper, B., He, X., Yankner, B.A., 1998. Destabilization of β-catenin by mutations in presenilin-1 potentiates neuronal apoptosis. Nature 395, 698–702.

Zhao, Y., Shen, L., Ji, H.-F., 2012. Alzheimer's disease and risk of hip fracture: a meta-analysis study. ScientificWorldJournal 2012, 872173.

Zhao, L., Liu, S., Wang, Y., Zhang, Q., Zhao, W., Wang, Z., Yin, M., 2015. Effects of curculigoside on memory impairment and bone loss via anti-oxidative character in APP/PS1 mutated transgenic mice. PLoS One 10, 1–13.

Zheng, H., Jia, L., Liu, C.-C., Rong, Z., Zhong, L., Yang, L., Chen, X.-F., Fryer, J.D., Wang, X., Zhang, Y., Xu, H., Bu, G., 2017. TREM2 promotes microglial survival by activating Wnt/β-catenin pathway. J. Neurosci. 37, 1772–1784.

Zhou, R., Deng, J., Zhang, M., Zhou, H.-D., Wang, Y.-J., 2011. Association between bone mineral density and the risk of Alzheimer's disease. J. Alzheimer's Dis. 24, 101–108.

Zhou, R., Zhou, H., Rui, L., Xu, J., 2014. Bone loss and osteoporosis are associated with conversion from mild cognitive impairment to Alzheimer's disease. Curr. Alzheimer Res. 11, 706–713.